Probabilistic Analysis of Maintenance and Operation of Artificial Recharge Ponds

Daniele Pedretti [a] Marco Barahona-Palomo [b] Diogo Bolster [c]
Daniel Fernandez-Garcia [a] Xavier Sanchez-Vila [a]
Daniel M. Tartakovsky [d]

[a] *Hydrogeology Group, Department of Geotechnical Engineering and Geosciences, Technical University of Catalonia (UPC-BarcelonaTech), 08034 Barcelona, Spain*

[b] *Hydrogeology Group, Department of Geosciences, Institute of Environmental Assessment and Water Research (IDAEA-CSIC), 08034 Barcelona, Spain*

[c] *Department of Civil Engineering and Geological Sciences, University of Notre Dame, Indiana, USA*

[d] *Department of Mechanical and Aerospace Engineering, University of California, San Diego, La Jolla, CA 92093, USA*

Abstract

Surface infiltration ponds (SIPs) are a popular approach to managed aquifer recharge in arid and semi-arid regions. We adopt a probabilistic approach to design the optimal schedule for maintenance of SIPs. It can be used to determine whether preventive measures aimed at maintaining the infiltration capacity constant are preferable to de-clogging, and to decide how often and to what extent the system must be regenerated (de-clogged). The latter decision involves tradeoffs between performing deeper (and more expensive) maintenance with low frequency and performing lighter (and cheaper) maintenance with higher frequency. Such decisions are site-specific and must be made under uncertainty inherent in siting, construction, and operation of SIPs.

Key words: managed artificial recharge, clogging, probabilistic risk analysis, infiltration rate

Email addresses: daniele.pedretti@upc.edu (Daniele Pedretti), dmt@ucsd.edu (Daniel M. Tartakovsky).

1 Introduction

Surface infiltration ponds (SIPs) are a popular approach to managed aquifer recharge (MAR) in arid and semi-arid regions [36,42]. Their effectiveness is determined in large part by infiltration capacity, $I[LT^{-1}]$, of the topsoil in which an SIP is to be constructed. It affects both the total volume of water that can infiltrate into the subsurface from the pond and the residence time of water within the pond, which control important chemical and biological reactions. The infiltration capacity at any given site is notoriously uncertain due to both soil heterogeneity and pore clogging. To complicate matters further, I is often estimated either directly (e.g., with infiltrometers [37]) or indirectly (e.g., from pore-or grain-size distributions [11,43]), introducing measurement and interpretive errors as well as the multiplicity of support volumes that can range from a few centimeters to several meters.

Inherent uncertainty in estimates of SIP's infiltration capacity and predictions of its temporal evolution introduces significant uncertainty into decisions about SIP's management, which can lead to economical and environmental losses. Management under uncertainty is properly formulated within a probabilistic framework context [23,32,45,48]. While risk analysis is a relatively new discipline in hydrogeology [4,8,38,39,20,46], it has become a standard practice in other engineering and environmental disciplines [31].

Although the infiltration capacity $I(\mathbf{x}, t)$ generally varies in space $\mathbf{x}$ and time t, the variable of interest in managing operations is its the spatially-averaged counterpart $\overline{I}(t)$. At a given time, it can be estimated either statistically from small-scale local measurements if sufficient amounts of spatially-distributed data are available, or experimentally with large-scale infiltration tests [1,3]. The temporal evolution of $\overline{I}(t)$—typically, its reduction—is caused by a combination of physical processes, which modify the properties of both the water and the soil. At a typical SIP site, one observes a significant reduction in porosity ϕ and permeability κ within the first few centimeters of the soil due to clogging [9,35]. Water temperature can be an important factor in biological clogging taking place over short time intervals [16]. Seasonal variations in the density and viscosity of water might contribute to the temporal variability of $\overline{I}$, but these effects are expected to be secondary and act on much larger time scales (months versus days associated with clogging).

Depending on the overall intensity of the clogging mechanisms, SIPs suffer from "aging" [30], i.e., from an appreciable reduction in the infiltration capacity $\overline{I}$, in the first few days after flooding. To meet the projected infiltration volumes, the system must be periodically maintained by adopting either preventive or corrective measures at different stages [2,13]. The speed with which $\overline{I}(t)$ approaches or drops below some critical threshold value I_c is the pri-

mary variable indicating when and what type of corrective measures should be taken.

In this paper, we adopt a probabilistic approach to design of the optimal schedule for maintenance of SIPs. Since the cost of maintenance depends on the frequency and type of maintenance, the proposed approach should include a cost-benefit analysis, which lies outside the scope of the present investigation. We use this methodology to evaluate if (and suggest which) preventive measures are preferable to corrective applications. It can also be used to decide how often and to what extent the system must be regenerated. Taking decisions about performing deeper (and more expensive) maintenance with low frequency or performing lighter (and cheaper) maintenance with higher frequency is strictly site-specific and must be made under uncertainty inherent in siting, construction, and operation of SIPs.

2 Operation of SIPs under Uncertainty

The complexity of modeling soil clogging and corresponding reduction in infiltration capacity, coupled with ubiquitously insufficient site characterization and soil heterogeneity, renders predictions of a pond's performance fundamentally uncertain. This challenge is partially alleviated by the fact that this performance is determined by the overall infiltration capacity $\overline{I}(t)$ rather than its point values $I(\mathbf{x}, t)$. The former is related to the latter by

$$\overline{I}(t) = \int_{\Omega} I(\mathbf{x}, t) \mathrm{d}\mathbf{x}, \tag{1}$$

where Ω is the area occupied by the infiltration pond. The empirical evidence from several operating SIPs [34] suggests an exponential decay in the overall infiltration capacity,

$$\overline{I}(t) = \overline{I}_0^* \mathrm{e}^{-\lambda_{\mathrm{eff}} t} \tag{2}$$

where the initial capacity $\overline{I}_0^*$ and the effective decay (clogging) rate λ_{eff} $[T^{-1}]$ are highly uncertain fitting parameters. One of the main goals of our study is to relate these parameters to soil properties and to physical, biological, and chemical mechanisms of clogging.

Different maintenance activities with different scheduling plans can be applied to a SIP to control the reduction of $\overline{I}$ with time [9,35]. These can be subdivided into preventive or corrective measures [7]. Preventive or maintenance activities are performed during the operation period in order to extend the system's life (time between two consecutive corrective measures). Corrective measures must be taken if and when $\overline{I}(t)$ reaches its minimally acceptable level I_c, and the SIP

operation must be stopped. Examples of the former include pre-filtering input water to eliminate particles, using disinfectants to control algae growing, and controlling entry water temperature to avoid gas bubbling. Examples of the former include scraping the bottom when the basins are dried out after specific recharge cycles, supplying additional disinfectants or chemicals to the water, and using underwater robots to scrape the soil surface during infiltration.

Regardless of the maintenance strategy under consideration, the system life is highly uncertain so that maintenance decisions have to be made under uncertainty, calling for a probabilistic approach. Instead, the current practice is to schedule reset operations (corrective measures) based on experience and monitoring [13]. An optimal scheduling and selection of maintenance measures affects the costs of operating SIPs. Forecasting these costs is subject to uncertainty and depends on many factors, such as the quality of the chemical products or the performance of the scraping machines.

3 Processes Contributing to SIP failure

Let I_c denote the smallest acceptable infiltration capacity of a SIP. We define "system failure" at time t as the event $\overline{I}(t) < I_c$. Among a large number of events that can lead to system failure [21] are interruptions in water supply to the pond deposition of extraneous impermeable materials at the pond's bottom, bad design and/or improper use of the pond, and its complete breakdown due to embankment slides, earthquakes, acts of vandalism, etc. These and other similar events should be included into a complete probabilistic risk assessment of SIPs, but lie outside the scope of the present analysis. Instead, we focus on the system failure due to reduction in the soil's infiltration capacity caused by clogging.

Clogging alters the hydraulic properties of a soil, leading to reductions in a SIP's infiltration capacity over time. A mathematical model capturing this phenomenon is presented in section 3.1. Alternative descriptions of various clogging mechanisms are discussed in section 3.2.

3.1 Infiltration & hydraulic parameters

In a well-designed SIP site, the top soil layer can be assumed to control infiltration. (A low-permeable layer, e.g., a clay layer with horizontal continuity, invalidates this assumption. The presence of such layers constitutes a design failure, and, hence, is not considered here.) Under this assumption, the top soil layer is (nearly) fully saturated and infiltration can be described by the

one-dimensional Darcy law,

$$I(\mathbf{x},t) = -K(\mathbf{x},t)\frac{\partial h(\mathbf{x},z,t)}{\partial z}, \tag{3}$$

where $\mathbf{x} = (x,y)^T$ is the horizontal coordinate vector, z is the vertical coordinate, h is the hydraulic head, and K is the saturated hydraulic conductivity. The latter is defined as $K = \kappa\rho_w g/\mu_w$, where κ is the soil permeability, ρ_w and μ_w are the density and dynamic viscosity of water, respectively; and g is the gravity acceleration constant. To account for changes in hydraulic conductivity due to pore clogging, we adopt the Kozeny-Carman law [29,12] according to which permeability κ varies with porosity ϕ as

$$\kappa = \frac{\phi^3}{k_s T S^2} = \frac{d_m}{180}\frac{\phi^3}{(1-\phi)^2} \tag{4}$$

where k_s is a geometrical factor, T is the tortuosity, S is the specific surface of the pores and d_m is the median percentile diameter.

Assuming that the water properties and the hydraulic gradient do not change with time, it follows from (3) that any reduction in infiltration capacity is linearly related to the reduction in K, i.e.,

$$\frac{I(\mathbf{x},t)}{I_0(\mathbf{x})} = \frac{K(\mathbf{x},t)}{K_0(\mathbf{x})}, \tag{5}$$

where $I_0(\mathbf{x}) = I(\mathbf{x}, t=0)$ and $K_0(\mathbf{x}) = K(\mathbf{x}, t=0)$ are the initial values of the infiltration capacity and the hydraulic conductivity, respectively. Combining (4) and (5), we obtain an equation relating the reduction in the infiltration capacity to the reduction in porosity,

$$\frac{I(\mathbf{x},t)}{I(\mathbf{x})} = \frac{\phi^3(\mathbf{x},t)}{\phi_0^3(\mathbf{x})}\frac{(1-\phi_0(\mathbf{x}))^2}{(1-\phi(\mathbf{x}))^2} \approx \frac{\phi^3(\mathbf{x},t)}{\phi_0^3(\mathbf{x})}, \tag{6}$$

where $\phi_0^3(\mathbf{x}) = \phi^3(\mathbf{x}, t=0)$ is the initial value of porosity before clogging started to occur. The zeroth order approximation in eq. 6 is valid whenever variations in ϕ are not very large.

3.2 Mathematical models of clogging

A number of physical [47], biological [6,19] and chemical [26] processes can contribute to clogging at a given site. Their complex interplay stymies the efforts to develop a comprehensive mathematical model of clogging even if an individual mechanism is well-understood [14,17,18,41]. Representative models of the three classes of clogging are discussed below.

3.2.1 Physical clogging

Physical clogging typically refers to filtration processes [28,47] that reduce porosity ϕ through sedimentation and dragging of suspended particles. Following [28], we employ a first-order mass transfer model,

$$\frac{\partial C(\mathbf{x}, z)}{\partial z} = -\lambda_z(\mathbf{x}) C(\mathbf{x}, z), \tag{7}$$

to describe the vertical (in z direction) profile of the volumetric concentration of particles, C $[ML^{-3}]$, that are removed from the suspension and get trapped within the soil. The filtration coefficient λ_z $[L^{-1}]$ represents volumetric and surface forces [34]. An exhaustive review of various forms of the filtration coefficient can be found in [47].

In a typical formulation, e.g., [10], λ_z is calculated as a combination of the following mechanisms. For filtration induced by inertial forces, $\lambda_{ine} \propto d_s^{1.5}$ where d_s is the mean diameter of suspended particles in the water during the flooding stage. For filtration due to interception mechanisms, $\lambda_{int} = (d_s/d_g)^n/d_g$ where d_g is a characteristic grain size of the soil, and the exponent n typically varies between 0.5 and 2.0. For filtration caused by molecular (van der Waals) forces, $\lambda_{mol} \propto d_s^2$. For filtration due to diffusion, $\lambda_{dif} = [\phi_0 K_b T/(\mu_w d_s d_g |q|)]^{0.66}/d_g$ where K_b $[L^2 M T^{-1\circ} K^{-1}]$ is the Boltzmann constant, T is the water temperature, and q $[LT^{-1}]$ is the flow velocity of water. For filtration due to sedimentation, $\lambda_{sed} = g\phi_0(\rho_k - \rho_w)d_s^2/(18\mu_w d_g|q|)$ where ρ_k is the bulk density of the soil.

Soil's characteristic grain size d_g affects its permeability κ. We choose d_{10}, the grain size that corresponds to the tenth percentile on the cumulative distribution of grain sizes in a given soil, to play the role of d_g and relate it to κ by employing the Hazen formula [27],

$$\kappa = A d_{10}^2, \tag{8}$$

where $A \approx 100$ is a geometrical coefficient that is typically related to the geometry of the sand. It should be noted that Hazen's formula (8) is strictly valid for clean sands and that its validity has been the subject of much debate. We employ it here to simplify the presentation, and other textural relations can be used instead. Finally, we assume that in SIP applications d_{10} doesn't change in time, i.e. that the clogging material doesn't affect the grain size distribution over time. Clogging materials are of order of magnitude smaller (in the case of suspended particle) or with less density (in the case of biomass) than the original material.

Let v_a denote an average particle's attachment velocity to the soil matrix. Typical values of v_a can be obtained from literature or from laboratory experiments. The experiments reported in [34] yield $v_a \approx 10^{-5}$ m/day, a value that

is in agreement with the reference values suggested in [40]. Setting $t = z/v_a$ in (7) and integrating in time yields

$$C(\mathbf{x}, t) = C_0(\mathbf{x})\mathrm{e}^{-\lambda_p^*(\mathbf{x})t}, \qquad \lambda_p^* = \frac{\lambda_z}{v_a}, \tag{9}$$

where C_0 is the initial concentration of particles in the soil column.

Changes in the concentration of particles δC cause changes in the porosity $\delta\phi$. We postulate a linear relation between the two, $\delta\phi/\phi = m_p \delta C/C$, where m_p is the coefficient of proportionality. It then follows from (9) that

$$\phi(\mathbf{x}, t) = \phi_0(\mathbf{x})\mathrm{e}^{-\lambda_p(\mathbf{x})t}, \qquad \lambda_p = m_p\lambda_p^*. \tag{10}$$

Substituting (10) into the approximation of (6) yields a model describing the exponential reduction in the infiltration capacity due to physical clogging,

$$I(\mathbf{x}, t) = I_0(\mathbf{x})\mathrm{e}^{-3\lambda_p(\mathbf{x})t}. \tag{11}$$

3.2.2 Biological clogging

Biological activity, such as biomass growth and biogas generation, obstructs the pores and reduces both porosity and pore connectivity [6]. Biological clogging is typically described with one of the three approaches: macroscopic model, micro-colonies-based models, and biofilm-based models. Macroscopic transport equations resulting from all three frameworks are identical if biofilms and micro-colonies are fully penetrating [5]. Furthermore, the three approaches yield acceptable predictions for coarse-textured materials (which are typically involved in SIP practices), while poor predictions are obtained for fine-textured materials [44].

Bio-clogging manifests itself through a formation of a thin impermeable layer at the soil surface, biofilm formation on the soil grains, and precipitation of biomass that occludes the pores in a whole. We will focus on the last two phenomena that act to reduce the porosity ϕ. Specifically, we adopt a macroscopic approach and assume that all biomass growth leads to a direct reduction of porosity, $\phi(\mathbf{x}, t) = \phi_0(\mathbf{x}) - \phi_b(\mathbf{x}, t)$, where $\phi_b(\mathbf{x}, t)$ accounts for the fraction of the pore volume that is occupied by the biological mass. This can be rewritten as

$$\frac{\phi(\mathbf{x}, t)}{\phi_0(\mathbf{x})} = 1 - \frac{\phi_b(\mathbf{x}, t)}{\phi_0(\mathbf{x})}. \tag{12}$$

Following [19], we express ϕ_b in terms of M_b $[L^3L^{-3}]$, the relative biomass

attached to the soil, via

$$\phi_b(\mathbf{x},t) = \frac{\rho_k(\mathbf{x})}{\rho_b} M_b(\mathbf{x},t), \tag{13}$$

where ρ_b is the biomass density.

In general, biomass growth occurs in four stages: time-lag (adaptation), exponential growth (microbes have acclimated), stationary (limiting substrate), and decay (substrate exhausted) [49]. While assessing the performance of SIPs, one is concerned with the initial stages of bio-clogging in which biomass grows exponentially,

$$M_b(\mathbf{x}) = M_b^*(\mathbf{x})[\mathrm{e}^{\lambda_s(\mathbf{x})t} - 1], \tag{14}$$

where $\lambda_s(\mathbf{x})$ is the growth parameter and $\lambda_s M_b^*(\mathbf{x})$ is the initial rate of growth of biomass. Combining (12)–(14) yields

$$\frac{\phi(\mathbf{x},t)}{\phi_0(\mathbf{x})} = 1 - \frac{\rho_k(\mathbf{x}) M_b^*(\mathbf{x})}{\rho_b \phi_0(\mathbf{x})}[\mathrm{e}^{\lambda_s(\mathbf{x})t} - 1], \tag{15}$$

which, for small t associated with the exponential biomass growth, can be approximated by

$$\frac{\phi(\mathbf{x},t)}{\phi_0(\mathbf{x})} \approx \mathrm{e}^{-\lambda_b(\mathbf{x})t}, \qquad \lambda_b = \frac{\rho_k M_b^* \lambda_s}{\rho_b \phi_0}. \tag{16}$$

It is worthwhile emphasizing that the approximation (16) is valid for small t, i.e., it implicitly assumes the variation in porosity due to biofilm growth to be small relative to the initial biomass. This assumption is adequate for risk assessment purposes, since a large reduction in porosity and permeability would make the SIP operation not viable. In other words, standard SIP operations would not allow clogging to develop beyond the exponential growth phase.

Substituting (16) into (6) yields a model describing the exponential reduction in the infiltration capacity due to biological clogging,

$$I(\mathbf{x},t) = I_0(\mathbf{x})\mathrm{e}^{-3\lambda_b(\mathbf{x})t}. \tag{17}$$

3.2.3 Gas clogging

During the pond filling, gas in pores can be generated by a number of chemical processes, including microorganisms activity, temperature effects, and release of trapped bubbles [15,24]. As the air replaces water in some pores (mainly large ones), water saturation and consequently hydraulic conductivity and infiltration rates decrease. On the other hand, in SIP degassing can be rapidly reversed if the proper water temperature conditions are met [34]. Since the relationship between moisture content and conductivity is characteristic of the

type of soil (i.e., of the grain size), gas clogging also show spatial variability in heterogeneous media. Direct measurements of the characteristic curves are challenging and costly.

Clogging due to gas formation takes place at a time scale that is much smaller than those associated with physical and biological clogging. Taking advantage of this fact, we employ an instantaneous reduction model of gas clogging,

$$I(\mathbf{x}, t) = R(\mathbf{x}) I_0(\mathbf{x}), \tag{18}$$

where the reduction factor $R(\mathbf{x}) \in (0, 1]$ is treated as an uncertain (random) fitting parameter.

3.2.4 Effective model of clogging

Assuming that the clogging mechanisms described above have a cumulative effect, the overall reduction in the infiltration capacity is obtained by combining (11), (17), (18),

$$I(\mathbf{x}, t) = R(\mathbf{x}) I_0(\mathbf{x}) \mathrm{e}^{-3[\lambda_p(\mathbf{x}) + \lambda_b(\mathbf{x})]t}. \tag{19}$$

4 Quantitative Assessment of SIP Performance

We adopt a probabilistic framework to predict the effects of clogging on a SIP's infiltration capacity, which is the most critical cause of operational failure. Section 4.1 contains a sensitivity analysis of the SIP infiltration capacity to various clogging mechanisms. In section 4.2, we use stochastic averaging to relate the point-wise uncertain infiltration capacity $I(\mathbf{x}, t)$ given by (19) to its effective counterpart $\overline{I}(t)$ in (2).

4.1 Sensitivity analysis

In section 3 we demonstrated how the reduction in the infiltration capacity $I(\mathbf{x}, t)$ in (19) can be related to the soil texture, to the soil particle size d_g. Here we explore further the question of how this soil parameter affects various clogging mechanisms and, via (19), the SIP infiltration capacity. In these simulations, we set $d_p = 2 \cdot 10^{-5}$ m, $n = 2$, $\rho_p = 1.5$ g/cm^3, $T = 298$ °K, $\rho_w = 1$ g/cm^3, $\mu_w = 1.002 \cdot 10^{-3}$ N sec/m^2, $K_b = 1.38 \cdot 10^{-23}$, $\lambda_s = 2.5 \cdot 10^{-3}$ 1/day, and $\rho_k = 1.8$ g/cm^3 for coarse soils, 1.5 g/cm^3 for mid-grained soils, and 1.2 g/cm^3 for fine soils. Finally, we fix $\phi_0 = 0.3$ and $q = 0.1$ m/day even though these parameters are expected to vary with d_g. This is done to isolate

the relative importance of the physical and biological clogging that depend exclusively on the grain size d_g.

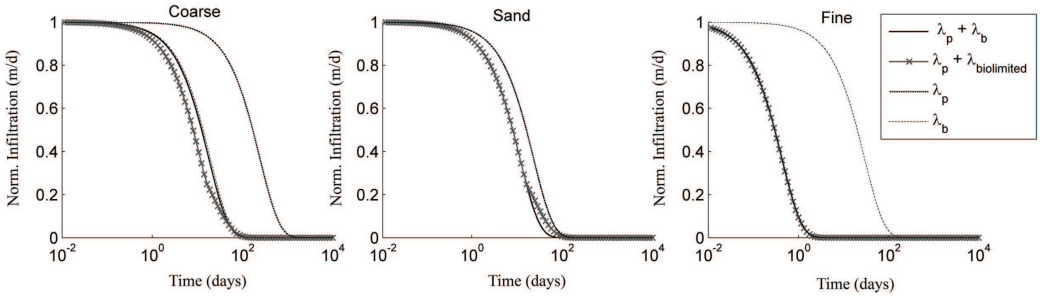

Fig. 1. Sensitivity on d_g of the temporal evolution of the infiltration capacity (normalized)

Figure 1 exhibits the temporal evolution of the infiltration capacity, normalized with its initial value RI_0 for d_g = **a, b, c** representing coarse sand, sand[**?**], and fine sand, respectively. For coarser soils, biological processes play the dominant role in soil clogging ($\lambda_p + \lambda_b$), while physical clogging plays a major role in fine-grained soils. For mid grain-sized soils, both mechanisms have similar intensities.

4.2 Probabilistic analysis

For heterogeneous soils, parameters R, I_0, λ_t, and λ_b can vary is space. As shown in section 3, all these parameters can be related to d_g. Let us assume that $d_g(\mathbf{x})$ incapsulates the spatial variability of these four parameters, so that (19) can be recast as

$$I(\mathbf{x},t) = \tilde{I}_0(d_g)\tilde{R}(d_g)\mathrm{e}^{-\tilde{\lambda}_p(d_g)t-\tilde{\lambda}_b(d_g)t} \equiv G[d_g(\mathbf{x}),t]. \tag{20}$$

We treat $d_g(\mathbf{x})$ as a random field whose ensemble statistics can be inferred from measurements taken throughout the SIP's footprint Ω.

To relate the point-wise infiltration capacity $I(\mathbf{x},t)$ in (20) to the total infiltration capacity $\overline{I}(t)$ in (2), we invoke the ergodicity hypothesis that postulate the equivalency between the spatial averaging, $\overline{I}(t)$, and ensemble averaging,

$$\langle I(t)\rangle = \int_{\mathcal{V}} G(s,t)p_{d_g}(s)\mathrm{d}s \tag{21}$$

where $p_{d_g}(s)$ is the probability density function of d_g defined over the event space $\mathcal{V}$. The effective clogging parameters in (2) can now be defined as

$$\lambda_{\text{eff}} = \frac{1}{t}\ln\left(\frac{\overline{I}_0^*}{\langle I(t)\rangle}\right), \qquad \overline{I}_0^* = \langle RI_0\rangle. \tag{22}$$

5 Applications

We demonstrate the salient features of the proposed approach on two examples. The first deals with field data collected at a pilot SIP site (section 5.1). The second considers several synthetic examples that enable one to analyze the approach's accuracy and robustness (section 5.2).

5.1 Pilot SIP in Sant Vicenç dels Horts, Spain

We use the mathematical framework developed in sections 3 and 4 to predict soil clogging and the corresponding reduction in the pond's infiltration capacity at a SIP site located in Sant Vicenç del Horts near the city of Barcelona, Spain. The site lies in the prodelta region of the Llobregat river, whose geology is a sequence of fine- and coarse-grained facies of silico-clastic materials, deposited according to the evolution of the paleoriver. The hydrogeological setting consists of sandy-gravel or gravelly-sand (depending on the proportion of the average grain sizes), separated by non-continuous fine-grained horizons. The SIP size is 45 m $\times$ 100 m, with excavation depth ranging from 4 m to 6 m below the ground surface.

Figure 2 presents an aerial photograph of the site. Heterogeneity (spatial variability) of the pond's surface material is clearly visible, and a series of double ring experiments [33] show that infiltration rates at different locations throughout the pond vary by orders of magnitude. Since the ground color depends on the soil texture, which in turn is correlated with the infiltration capacity, the ground color in Fig. 2 was used [33] to infer the point-wise infiltration capacity $I_0(\mathbf{x})$ throughout the pond (Fig. 3A). The authors found the local measured infiltration rates to be linearly correlated with the logarithm of the pixel intensity of the satellite image in Fig. 2 (which happened to have approximately the same measurement support).

Figure 3B exhibits the characteristic grain size distribution $d_g(\mathbf{x})$ inferred from the distribution of $I_0(\mathbf{x})$ in Fig. 3A by means of the Hazen formula (8). The logarithmic color scales in Fig. 3 highlight the high degree of spatial variability present in the SIP. The parameters are inferred, and assumed to be constant, on a pixel basis (the size of the image is 286 $\times$ 694 pixels).

The inferred values of characteristic grain sizes $d_g(\mathbf{x})$ are next used to estimate the physical clogging rate λ_p by following the procedure described in section 3.2.1. Figure 4A presents the spatial distribution of the physical clogging rate λ_p resulting from this procedure. Note that the λ_p values span four orders of magnitude.

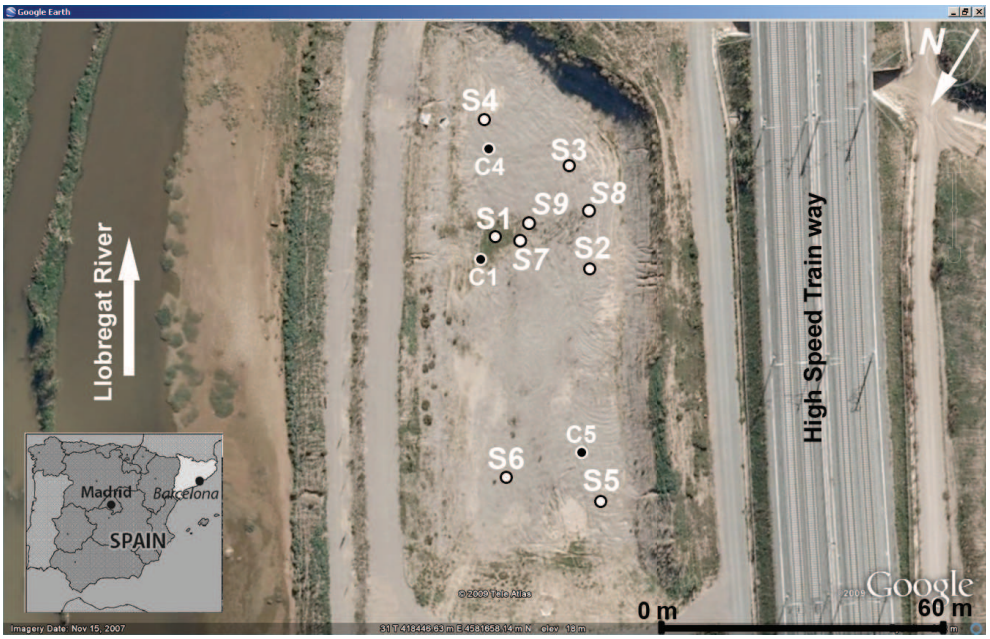

Fig. 2. A satellite image of the Sant Vicenç dels Horts site (from Google Earth).

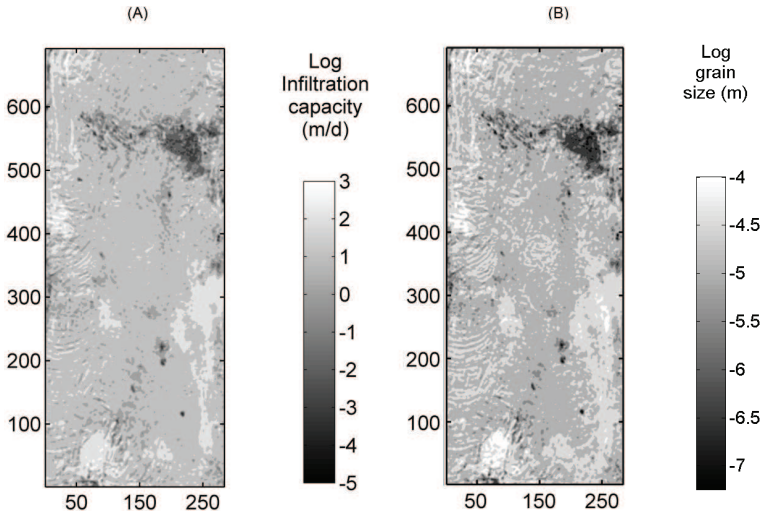

Fig. 3. (A) Infiltration capacity distribution after initial flooding (modified from [33]), and (B) corresponding relative grain-size distribution predicted with the Hazen formula (8).

Next, we use the inferred values of characteristic grain sizes $d_g(\mathbf{x})$ to estimate the biological clogging rate λ_b by following the procedure described in section 3.2.2. In doing so, we set $\lambda_s = 2.4067 \cdot 10^{-5}$ and $\rho_b = 2.5 \cdot 10^{-3}$ g/cm^3. To compute values of $\rho_k(\mathbf{x})$, which depends on $d_g(\mathbf{x})$, we use a discrete subdivision

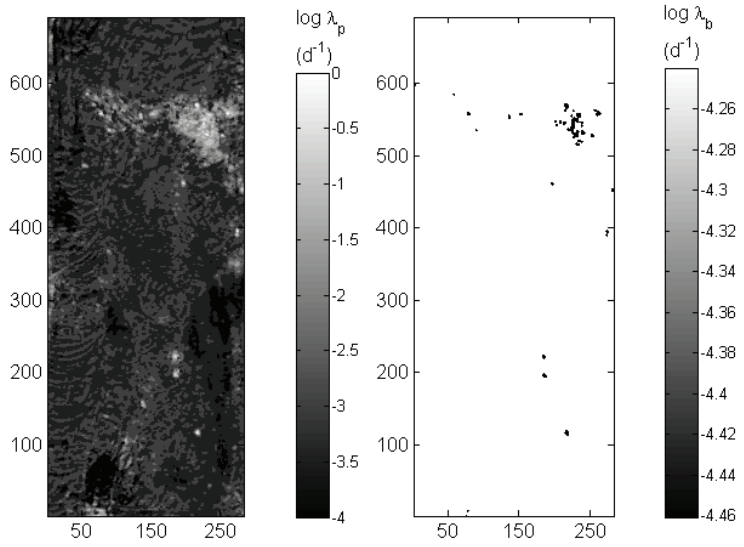

Fig. 4. Spatial distributions of (A) the physical clogging rates λ_p and (B) the biological clogging rates λ_b.

of the map in Fig. 3B,

$$\rho_k = \begin{cases} 1.8 & d_g \geq 1.5 \\ 1.5 & 1.5 \cdot 10^{-2} \leq d_g < 1.5 \\ 1.2 & d_g < 1.5 \cdot 10^{-2}. \end{cases} \tag{23}$$

Here the units of d_g and ρ_k are cm and g/cm^3, respectively. The spatial distribution of the biological clogging rate λ_b computed with this procedure is shown in Fig. 4B. One can see that λ_b is nearly constant of the surface of this SIP.

Assuming that the reduction factor R due to chemical clogging is spatially homogeneous and equal to $R = 0.9$ and substituting the distributions of λ_p and λ_b from Fig. 4 into (19), we compute the infiltration capacity $I(\mathbf{x}, t)$ in each pixel. Temporal snapshots of the resulting $I(\mathbf{x}, t)$ after 7, 14 and 42 days of infiltration are shown in Fig. 5. Comparing these snapshots with the initial infiltration capacity in Fig. 3A reveals the signification deterioration in the SIP performance. After 7 days many of the high capacity infiltration regions persist, while after 42 days the amount of high infiltration regions is significantly reduced.

A histogram (probability density function or pdf) and the corresponding cumulative distribution function (cdf) of the infiltration capacity after 7, 14 and 42 days are shown in Figs. 6. At early times there is a broad distribution of infiltration capacities. As time increases the PDFs shift to the left reflecting the decrease in infiltration rates and become narrow indicating smaller variability (uncertainty). They do so while maintaining tails at relatively high values of

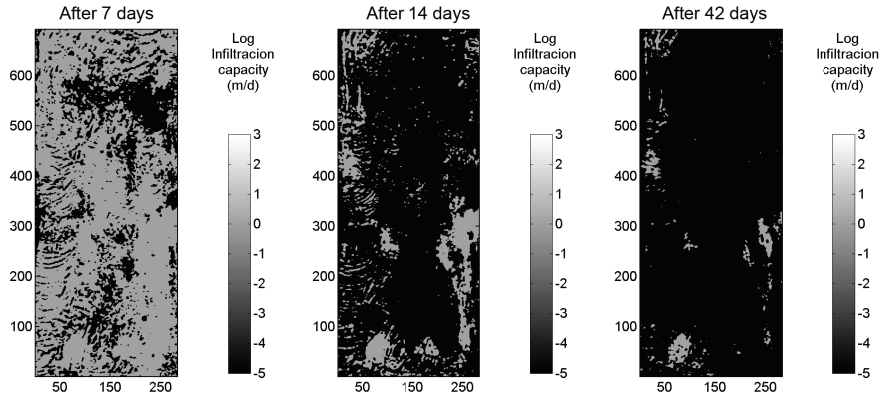

Fig. 5. Infiltration capacity of the soil at different flooding stages at the Sant Vicenç dels Horts site obtained from 19 from the initial infiltration value (fig. 3A) and the map of λ values (fig. 4), and assuming a constant reduction factor

infiltration (this is particularly evident in the cumulative densities). If there were some manner of optimally maintaining higher infiltration rates such that these tails were larger one could maintain larger mean infiltration capacity over longer periods of time, thus increasing the SIP's useful operational time.

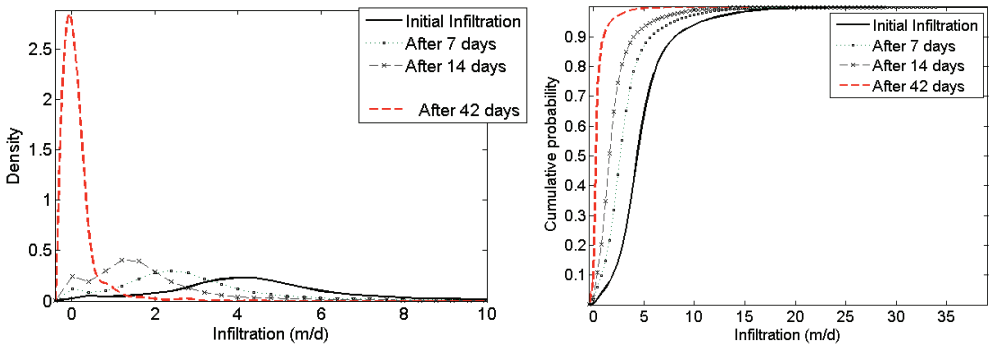

Fig. 6. (A) Histogram and (B) cumulative distribution function of the pixel-wise infiltration capacities $I(\mathbf{x}, t)$ estimated at 7,14 and 42 days after operation at the Sant Vicenç del Horts site.

While the spatial variability of the infiltration rate may be interesting, from a purely practical perspective the quantity that matters most is the average (total) infiltration rate $\overline{I}$ as it quantifies the actual total amount of recharge taking place. It is obtained by averaging (19) over all the pixels. The resulting $\overline{I}(t)$, normalized with initial infiltration capacity $\overline{I}_0^*$, is shown by the solid lines in Fig. 7. Recall that both (17) and (19) ignore the existence of the maximum threshold of biological growth, i.e., assume that the exponential growth/bio-clogging continues indefinitely. The dashed lines in Fig. 7 represent $\overline{I}(t)$ that accounts for biolimiting effects by impose a threshold for maximum biological growth in accordance with [19]. The relative difference between the two models may be considered significant at later times, with the biolimiting model predicting the infiltration capacity twice as large as the non-limiting

case after 35-40 days. However, the SIP's operation would cease much earlier, since the reduction of the infiltration capacity to 10% of its initial value is clearly unacceptable.

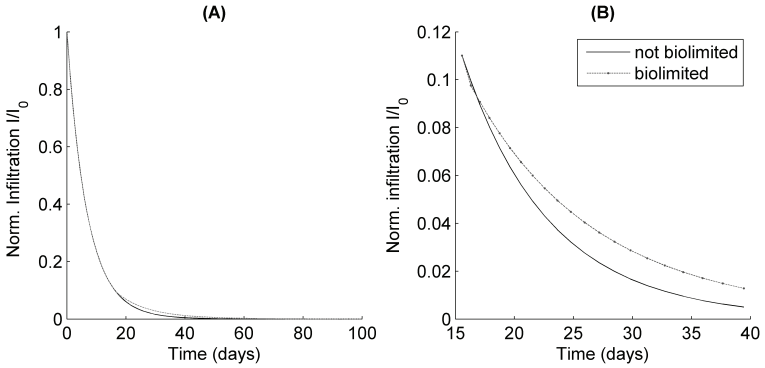

Fig. 7. Predicted reduction in the overall infiltration capacity $\overline{I}$ of the SIP at the Sant Vicenç del Horts site. Curves in Fig. 7B are a magnification of their counterparts in Fig. 7A over a shorter time interval. The dotted lines incorporate the biolimited process.

Finally, we investigate the applicability of the concept of λ_{eff}, the effective clogging rate that quantifies the rate of clogging over the whole domain and incorporates the variability of clogging mechanisms. As defined by (22), λ_{eff} can vary in time, reflecting the fact that the ensemble (or spatial) averaging does not automatically eliminate time dependence. However, numerical evaluation of (22) with the $\overline{I}(t)$ shown in Fig. 7 results in $\lambda_{\text{eff}} \approx 0.139$ that is practically constant in time. The best fit of the data averaged on a pixel per pixel basis (e.g., the data in Fig. 7) results in an exponential curve and an estimated clogging rate of $\lambda_{\text{eff}} = 0.143$ with a relative error three orders of magnitude smaller than the predicted value (see Fig. 8). The close agreement between the best fit and the theoretical model (22) is encouraging since it helps to explain why the reported mean infiltration rates in real artificial recharge ponds have been observed to follow a "homogeneous" exponential decay (e.g., [22]).

While the total infiltration capacity $\overline{I}(t)$ is the most important characteristic of a SIP site, information about the point-wise infiltration capacity $I(\mathbf{x}, t)$ might be used to maintain higher levels of infiltration over longer periods of time by effectively treating or maintaining the SIP to mitigate the clogging effects. In what follows, we demonstrate how efforts related at reducing specific clogging mechanisms can help to increase mean infiltration. We focus on four types of maintenance:

- No maintenance activity is performed,
- All biological clogging mechanisms are remediated (Type A),
- All physical clogging mechanisms are remediated (Type B),
- Physical clogging mechanisms are remediated in a part of the SIP footprint

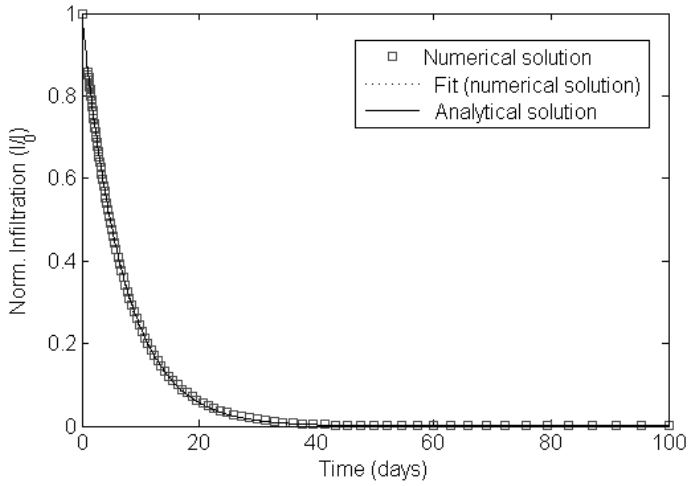

Fig. 8. Exponential decay in the overall infiltration capacity predicted with the three alternative models of clogging.

(Type C).

The Type C maintenance might employ different criteria to identify the parts of the SIP footprint where the remediation is to take place. One could clean an area selected purely on geometrical criteria (e.g., target a half of the area of the pond at a time). We pursue a different Type C maintenance strategy that is based on soil heterogeneity and hydraulic criteria to select clean-up areas. Specifically, we aim to target areas in which λ_p (Fig. 4A) fall below a certain threshold value, e.g., 50% or 80% percentiles of the λ_p probability distribution (Fig. 9). Since $\lambda_p \propto I_0^{-1}$, such maintenance strategies focus on the areas with the highest initial infiltration capacity I_0, aiming to sustain higher infiltration rates for longer and thus increasing the mean infiltration capacity over longer times. Unfortunately, complex geometries over which such a maintenance is to be performed suggest practical difficulties with its implementation.

Figure 10 displays the average infiltration capacity $\overline{I}(t)$ achieved with the four maintenance strategies identified above. Not surprisingly, all the strategies increase $\overline{I}(t)$ relative to its counterpart without any maintenance. If one defines 37% of the initial infiltration rate (which approximately equals the characteristic time $1/\lambda_{\text{eff}}$) as the minimum acceptable infiltration capacity, then the SIP's operational time without maintenance is about 7 days. Treating bio-clogging extends the operational time to about 9.5 days, and the full treatment of physical clogging increase the operational time to about 28 days. This highlights that physical clogging is the primary inhibiter for maintaining effective mean infiltration rates.

If only partial maintenance of physical clogging is performed, a treatment of 50% of the domain extends the operational time to 18-20 days. A more extensive treatment, 80% of the domain, delivers a substantial gain over the

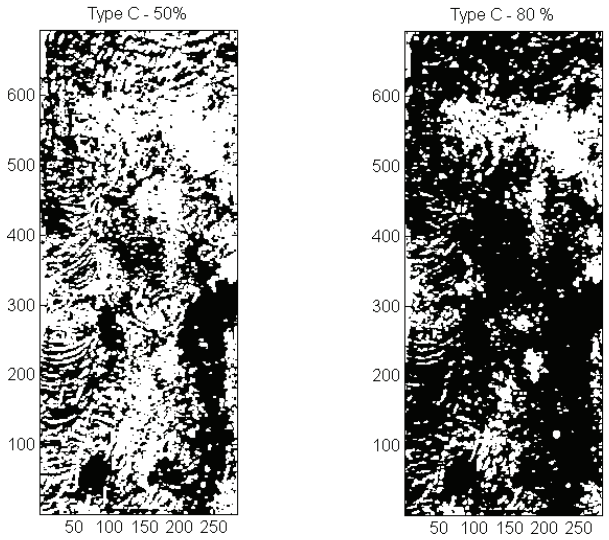

Fig. 9. Areas of applications of the Type C maintenance (in black) corresponding to the 50% (left) and 80% (right) percentiles of the biological clogging rate λ_p.

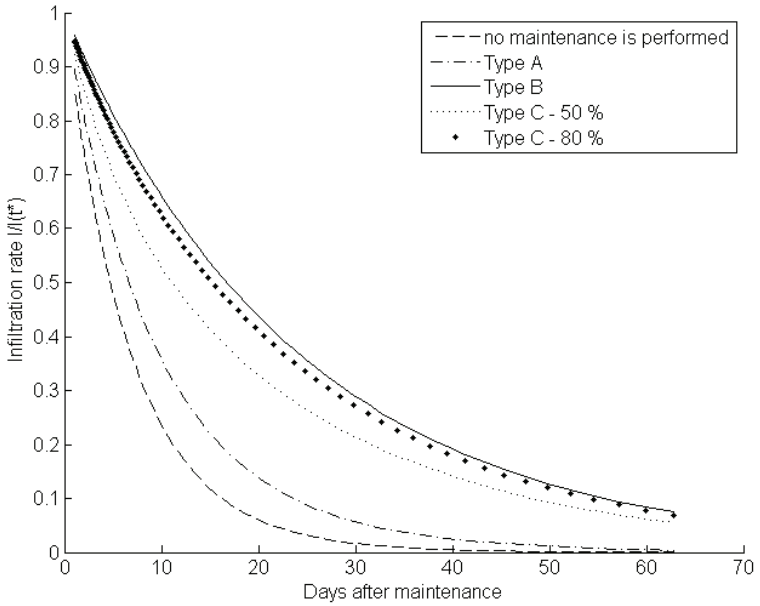

Fig. 10. The overall infiltration capacity $\overline{I}(t)$ of the Sant Vicenç del Horts SIP corresponding to different types of maintenance.

untreated case of about 25-27 days. Thus, if feasible, partial targeted maintenance offers significant gains in operational time.

5.2 Synthetic heterogeneous soils

To explore the effects of spatial variability in the parameters r, I_0, R, λ_b and λ_p, we supplement our analysis of the Sant Vicenç del Horts SIP with similar analyses on other possible geometrical distributions of hydraulic parameters. We build several synthetic multigaussian fields of heterogeneous distribution of the natural logarithm of the hydraulic conductivity ($Y(\mathbf{x}, t_0)$ =ln($K(\mathbf{x}, t_0)$)). Y has units of meters per day. Analogously to the Sant Vicenç del Horts, t_0 is the time when the maintenance is performed. We maintain the size of the computational domain as that of real case analysis (284 $\times$ 692 pixels). The random fields were generated using a sequential simulation algorithm [25], and are unconditioned to hard data. All fields have been built assuming an exponential variogram, mean zeros ($\overline{Y}(t_0) = 0$), different variances σ_Y, and correlation lengths, I_S.

We start by analyzing a single realization and then evaluating several realizations as an ensemble within a Monte Carlo (MT) framework. In the first case, the focus is to make a direct comparison between the real case of Sant Vicenç del Horts and another possible soil configuration where the spatial distribution of $Y(\mathbf{x}, t_0)$ is fully known (for instance, in the case of availability of reliable secondary information). On the other hand, the MT analysis generalizes the results accounting for a completely random generation of $Y(\mathbf{x}, t_0)$ in order to evaluate the spatial uncertainty due to the non-ergodocity of certain field geometry.

5.2.1 Results of single realization analysis

For illustrative purposes, we generated four unconditional fields of four selected types of spatial organization of $Y(\mathbf{x}, t_0)$. Such fields are shown in Fig. 11. Field 1 has σ=4 m^2/day^2 and I_s=66 pixels, Field 2 has σ=4 m^2/day^2 and I_s=6.6 pixels, Field 3 has σ=1 m^2/day^2 and I_s=66 pixels, and Field 4 has σ=1 m^2/day^2 and I_s=6.6 pixels.

Figure 12 shows how different maintenance strategies affect the decay in the infiltration capacity of the four fields. The Type C maintenance is based on the 50% of the distribution of λ_p (the value differs from field to field). Results are normalized in the same manner as for the previous case. Many features are similar to those observed in the previous case. Biological clogging always plays a secondary role compared to physical clogging. When physical clogging is removed, the four mean infiltration curves are virtually identical. This suggests that the impact of soil heterogeneity on the biological processes is very weak, while its influence on physical clogging is significant.

Spatial correlation of the infiltration capacity, I_s, is an important parameter

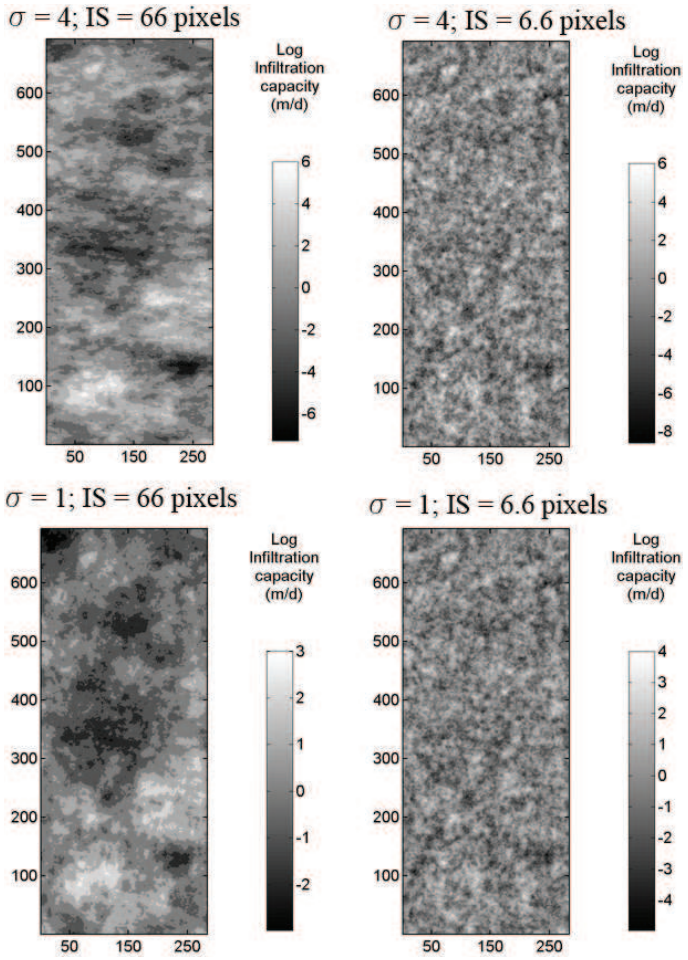

Fig. 11. Synthetic distributions of the initial infiltration capacity $I_0(\mathbf{x})$ corresponding to different variances σ_Y and correlation scale I_s.

affecting the SIP's performance. For the large correlation length (I_s =66 pixels, right figure), increasing σ_Y four-fold does not change the overall results significantly. Type A and B maintenance curves almost overlap, as do the curves corresponding to no maintenance cases. Only the targeted physical clogging activity (Type C) is different. For the short correlation length (I_s =6.6 pixels, left figure), the maintenance effectiveness is much more sensitive to σ_Y. The targeted (Type C) maintenance offers the biggest gains when the variance is large (reflecting the nonlinear scaling of physical clogging mechanisms). While the relative gain is smaller, treating bio-clogging by the Type B activity also offers a gain in performance for the larger variance field.

5.2.2 Results of Monte Carlo analysis

In the optic of risk evaluation for soil engineering practices, quantifying the uncertainty derived from the randomness of the spatial distribution of hydraulic parameter is a necessary step. To do it, we performed a Monte Carlo analy-

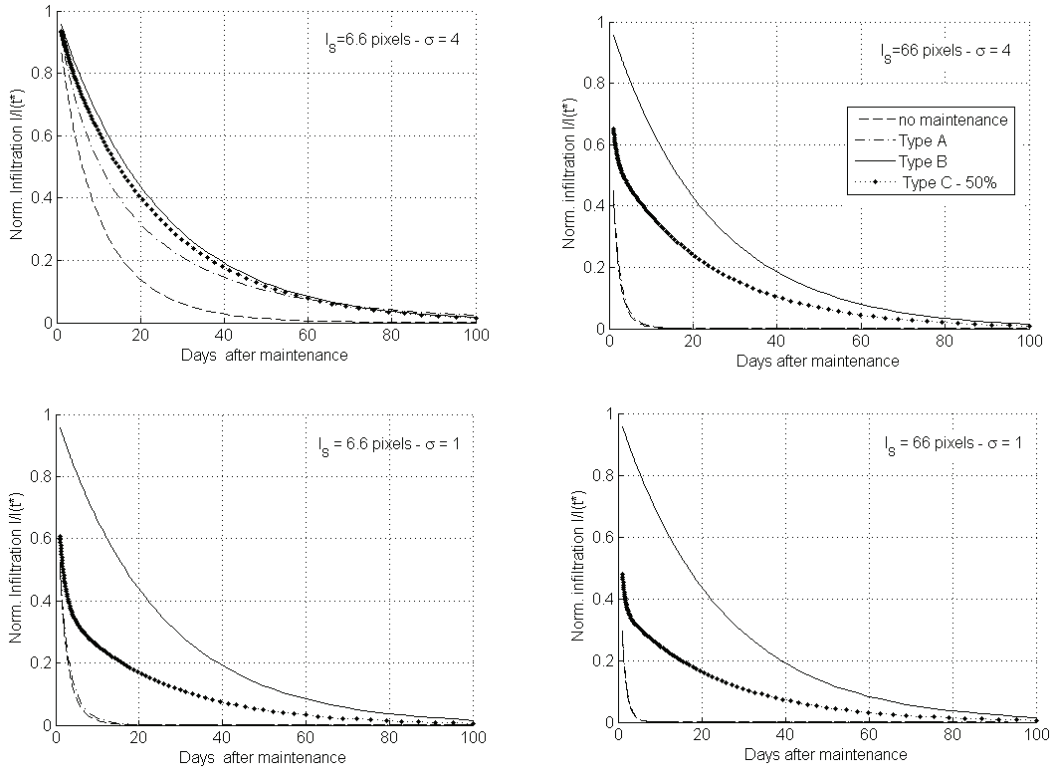

Fig. 12. The normalized overall infiltration capacity $\overline{I}(t)$ of the four synthetic SIP sites corresponding to different types of maintenance.

sis on 1000 additional unconditioned realizations of the previously generated fields (Section 5.2).

Fig. 13 and fig. 14 display some of the most significant results resulting from the analysis. The first figure represent the change over time of the spatial-averaged infiltration capacities ($\overline{I}(t)$), in log scale. The thicker lines correspond to the ensemble mean of the realizations, while the thinner lines are confidence intervals, which are expressed as the 95% of the normalized errors. Within fig. 13, the left plot refers to the fields with the highest I_S (66 pixels) and highest σ_Y (4 m^2/day^2); on the right side, the upper plot represents the case of high variance but lower correlation scales. The left-mid and left-lower plot correspond to the case with $\sigma_Y = 1$ m^2/day^2, and respectively with longer and shorter correlation of Y. The confidence bounds get narrower as I_S and especially σ_Y decrease. For this reason, we do not plot them for the case of σ_Y=1 m^2/day^2, as they practically match the ensemble mean.

We notice that, for high σ_Y, maintenance of type A (biological treatment) has in general long-term better benefits than the other maintenance systems, even if it is very uncertain when I_S is larger (meaning that it can be either extremely efficient or extremely poorly efficient). On the other hand, the uncertainties reduce as I_S diminishes. As the soil gets more homogeneous (lower

σ_Y), physical treatments (type B and C) give considerably more benefits than biological treatment (type A). The selection of one specific method is discussed in the following section.

The soil configuration and the spatial distribution of the initial local infiltration capacities ($I(\mathbf{x}, t_0)$) also control the type and intensity of the maintenance activity. This is reflected in the temporal change of the shape of the frequency distribution of the infiltration values during the recharge process. Fig. 14 report the experimental cumulative distribution frequency (CDF) of $\overline{I}(t)$, normalized on $\overline{I}(t_0)$), calculate for each realization at five time stages t_1 to t_5, which correspond to 1 day, 7 days, 14 days, 21 days and 42 days after the soil recovering (t=0). The normalization make the initial CDF being a unit-step function at t=0. According to fig. 13, in most cases, the CDFs maintain a step-like shape throught the observed recharge time; nonetheless, it is more sensitive to time changes when fields show higher σ_Y-I_S (for which the uncertainty, or the spreading around the temporally varying ensemble median value, also increases quicker) than for the cases with lower σ_Y-I_S.

Important information can be also obtained by observing the shape that the frequency distributions assume during the recharge time. From fig. 14 it seems that the cdfs tend to change from symmetric to asymmetric distributions; this behavior is especially pronounced in case of maintenance of Type A as well as for higher I_S-σ_Y combinations. We analyze the probabilistic density functions (PDF) for these specific cases as a useful way to highlight such patterns. The PDF are calculated as the best-fitted approximation to the discrete experimental histograms of infiltration capacities distribution. In fig. 15 we plot the PDF for different types and intensities of maintenance activities, considering also the case of no maintenance, calculated for a selected soil configuration (I_S = 66 pixeles and σ_Y = 4 m^2/day^2) at three different time stages (t_2, t_3 and t_5). Fig. 16 shows, on the other hand, the PDFs relative to different soil configurations assuming that only Type A of maintenance is applied. For t_2 and t_3 we fitted an equivalent normal distribution, while for t_5 we fitted a log-normal distribution. Notice that in most cases the discrete distributions tend to a Dirac function; thus, it has not been calculated for these cases. In fig. 15, the fitting process is not applied for the Type C case as the shape of the histograms is clearly different from both normal and log-normal distribution (they are negatively skewed). This is due to the fact that the type C select only certain portion of the domain, keeping higher frequency of higher values of $I(\mathbf{x}, t)$ and thus maintaining higher statistical mean infiltration capacity.

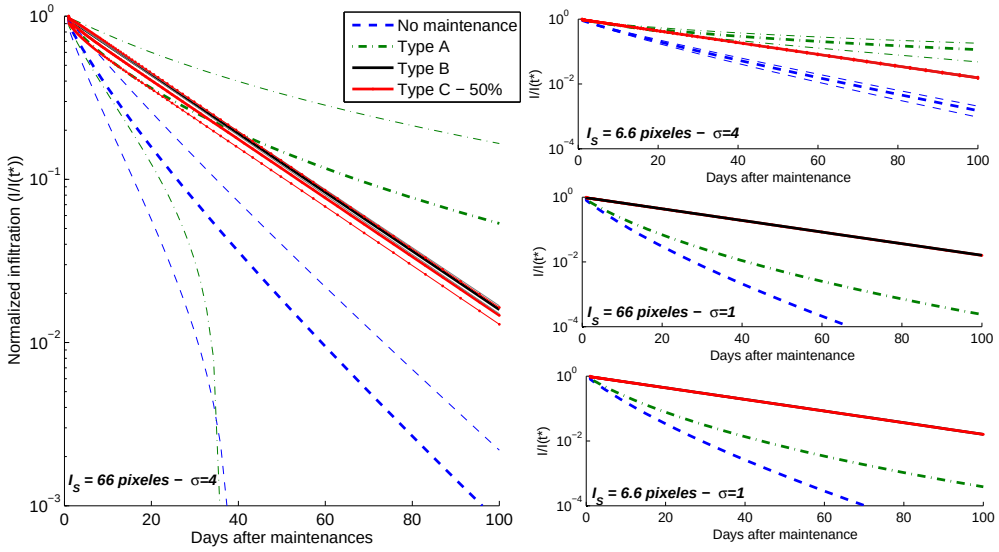

Fig. 13. Ensemble average (thicker marks) resulting from Monte Carlo analysis and corresponding 95% interval confidences (finer marks) of the normalized overall infiltration capacity $\overline{I}(t)$ in time for each field geometry and variance, for different types of maintenance. Notice that the vertical axis is set in logarithm scale. As the confidence intervals become narrower (and irrelevant from a practical point of view) for $\sigma = 1$, the figure displays only the ensemble average for such variance.

6 Discussion

The analysis offer a wide range of possible options to perform soil maintenance depending on the initial soil configuration, and to the degree of geological characterization. The most important results is that the efficiency of a specific method is related to the hydraulic heterogeneities, or better said to the degree of homogenization and organization of a soil. It should be noticed that these results are purely modelling-driven results. In the practice, selecting one of the maintenance methods is strictly site-specific and should be based on a local cost-benefit analysis. Such analysis accounts for the local availability of specific tools for clogging removal, the technical support, the availability of selected type of water, the extension of the recharge fields area, and many other terms. For instance, one maintenance method can be extremely cheap with regards to the others, and thus its applicability could be made with higher frequency in order to prevent the soil for clogging. Our analysis indicate that, from a technical point of view, the uncertainty of the de-clogging method is extremely site-dependent. The results give raise to some considerations, that are listed as follow.

1) In the real case analysis, the initial distribution of the local infiltration capacity is quite symmetric even if not parametric (fig. 6. The synthetic fields

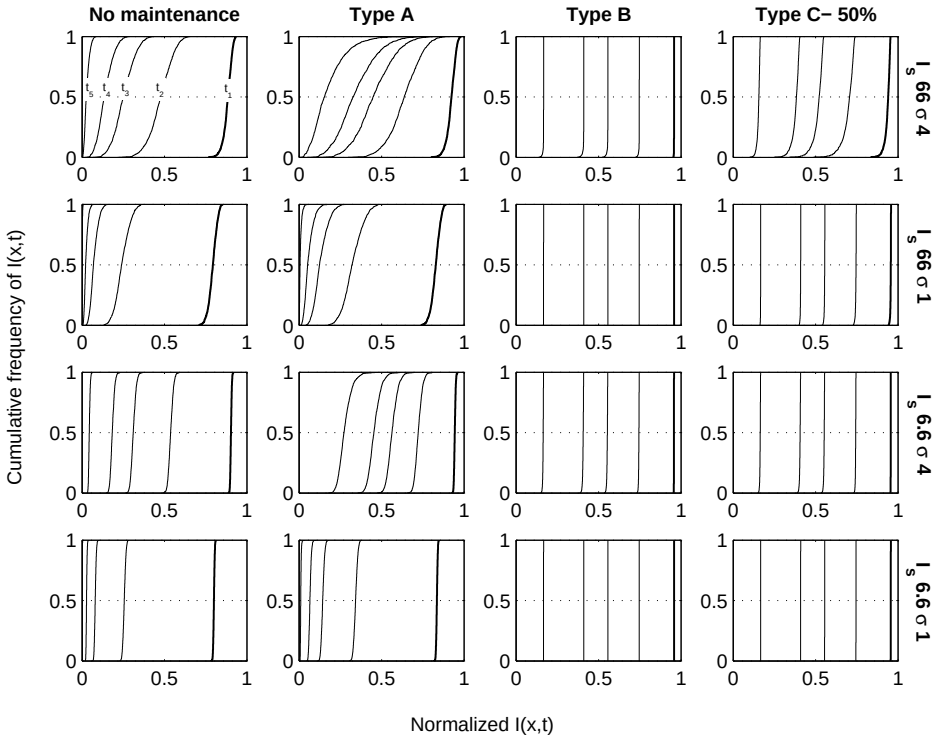

Fig. 14. Cumulative distribution frequency (cdf) of the normalized overall infiltration capacity $\overline{I}(t)$ resulting from the Monte Carlo analysis.The selected times consider t_1=1, t_2=7, t_3=14, t_4=21 and t_5=42 days after the maintenance operations. In each plot, the thicker line indicates t_1. Notice that the rate at which time evolution of the mean value (cdf = 0.5) changes depending on the soil configuration and the type of maintainance. The shape of the curves also changes over time, and is more sensible for fields with higher I_S and σ_Y, and especially for applications on bioclogging (Type A).

were generated, on the other hands, using a Gaussian simulator. In both cases, the tendency is to achieve an asymmetric log-distribution as the recharge is applied. This is especially visible observing the Monte Carlo outputs for Type A of maintenance, or by assessing the case with high σ_Y and I_S.

2) Uncertainty is extremely related with the soil homogenization. In the multigaussian fields of Y (the natural logarithm of K), the equivalent distribution of the grain size (calculated using the Hazen model) is also log-normal. Therefore, the higher σ_Y, the higher the probability to encounter fine materials. Type A maintenance eliminate all biological clogging mechanisms, so that clogging depend only on the physical mechanisms. Since the latter are more sensitive to finer grain size (low d_g) than for coarser grain size (high d_g) (fig. 1), increasing the probability to encounter low d_g values arises the sensibility of the CDF to change over time. For type of maintenance B and C, biological-treatment benefits generally dominate, and since they are practically not sensible to d_g (with this initial configuration of distribution of Y), the shape of the CDF do

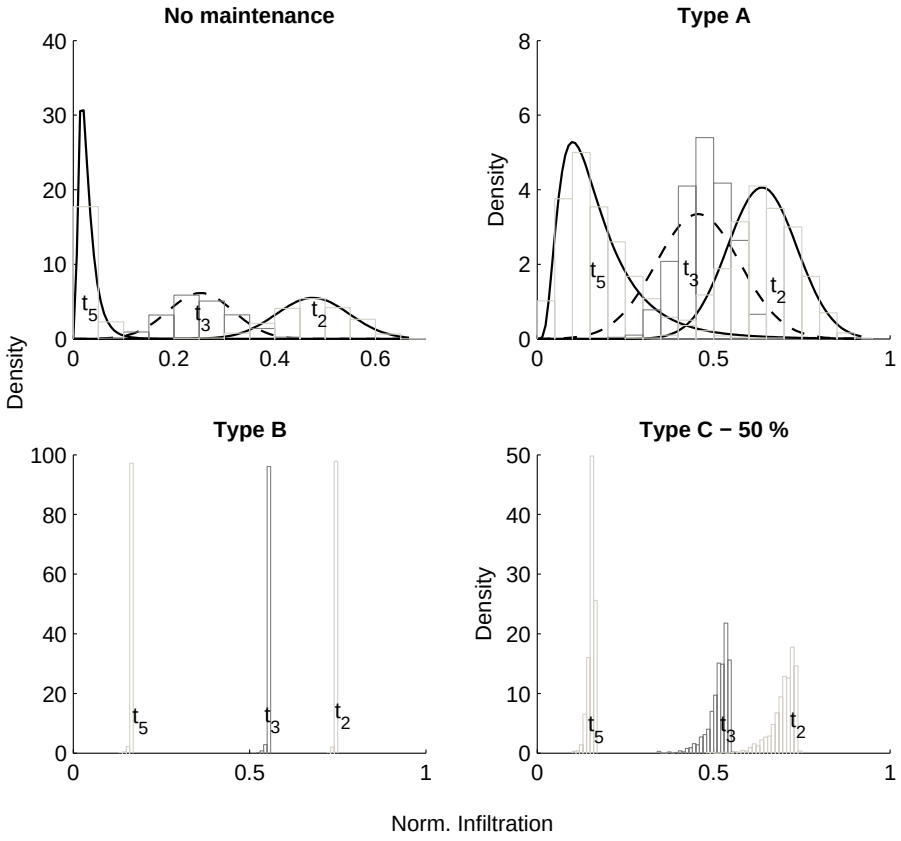

Fig. 15.

not change significantly in time.

3) The uncertainty is also related to the correlation scales, to the stationarity of the process and to the ergodicity of the solution. The relationship between the domain size and I_S diminishes as the latter term increases, meaning that less heterogeneity is explored over the same number of realizations. The result suggests that special care must be taken when upscaled groundwater models are used as a support tool for taking decisions on the SIPs. If the selection of an effective K to model a whole domain is obtained, for instance, relating σ and the correlation scales (which is a typical and well known approach e.g. Sudicky 1986, Dagan 1989, Matheron, 1967, Rubin, 1993), one could in principle hide the essential dependency of the type of maintenance upon one of the two parameter.

4) Fig. 9 indicates the zone of the real case where maintenance should be performed in order to recover the mean infiltration; being these zones quite extended and recognizable, maintenance activity of type C can be easily performed. Therefore, we suggest to include a geometrical factor (for instance, the I_S) to properly formulate the risk, in order to account for uncertainty of properly highlighting the zones where to perform the maintenance activity.

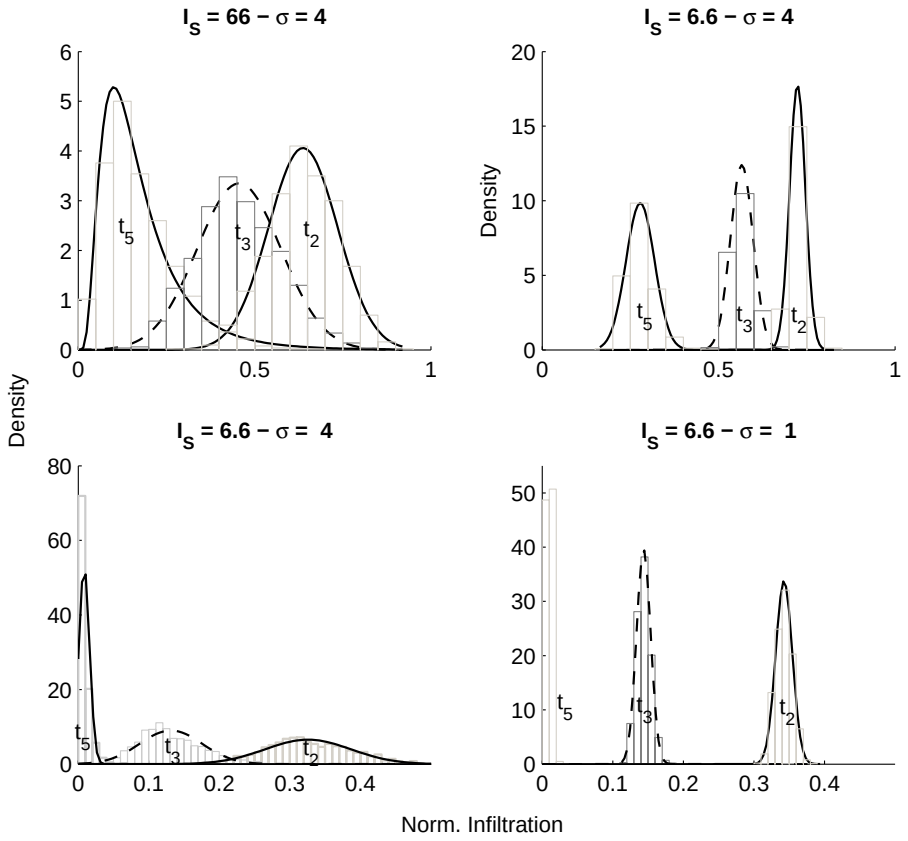

Fig. 16. C

5) Properly performed geological characterizations are fundamental for optimum cost-benefit analysis and design of maintenance activities on SIP. This especially true in the cases of great variability of soil parameters in small-scale sites (like the typical infiltration ponds). In the single realization analysis we analyzed two cases where the spatial distribution of hydraulic parameters (in specific, $I(\mathbf{x}, t)$) was supposed to be fully known at each portion of domain. Nonetheless, in many practices this is not always possible, especially where geological characterization lacks and no exhaustive secondary information exists. On the other hands, the Monte Carlo simulations are completely unconditioned to any local measurements of $I(\mathbf{x}, t)$. In this sense, this is the opposite case of the previous analysis (full spatial knowledge). In the practice, a (typically, limited) number of field measurements is normally available, and in principle could reduce the degree of uncertainty about the selection of a specific clogging method.

Conclusion

An effective use of Surface Infiltration Ponds (SIPs) requires maintaining the soil to recover the infiltration capacity after certain type has elapsed after the pond has been flooded. Recovering means maintaining specific amount of the overall infiltration capacity at the facility scale. Of the many processes that affect infiltration, clogging typically play the leading role. Soil heterogeneity at SIP sites induces spatial variability of both local infiltration rates and local clogging parameters, which complicates the accurate predictions of mean infiltration (averaged over the whole pond). In this work we developed a probabilistic framework to evaluate the risk of taking decision about how to manage a SIP under uncertainty. The framework focuses on physical, biological and retardation-like clogging mechanisms, although additional processes can easily be included. We demonstrate that physical clogging (strictly related to some typical parameter of the soil like the grain size) is most sensitive to soil heterogeneity rather than the biological treatment. We applied our general methodology to two sets of single realization examples (a real SIP and four synthetic ones), and within a Monte Carlo framework. The single realization approach (where we considered the spatial distribution of the initial infiltration capacity to be fuilly known at any location of the pond) demonstrates how a heterogeneous system, where local infiltration rates can range over several orders of magnitude, can be described with an effective homogeneous decay rate, a fact that has been observed at several field sites. The Monte Carlo framework shows that the risk of taking optimum decisions depends on the soil heterogeneity. Uncertainty mainly depends on the global variability of the hydraulic property of the soil (risk increases as the variance of the hydraulic conductivity increases). The geometrical distribution (evaluated by the correlation scales) of such parameters plays a secondarily role. These results suggest that the geological knowledge of the soil (thus, the geological characterization) is determinant for the optimum decision of maintenance operation on the SIPs. In any case, a cost/benefit analysis would have to be performed considering the costs and feasibility of such activities.

Acknowledgment

This study was originated at a workshop/class taught by DMT at the Technical University of Catalonia. It was sponsored by the Generalitat de Catalunya. We acknowledge the financial support of the Spanish Ministry of Science and Innovation via the 'Juan de la Cierva' , the CONSOLIDER-Ingenio 2010 (CSD2009-00065), RARAAVIS (CGL2009-11114) and HEROS programs. The work of DMT was supported by the Office of Science of the U.S. Department of Energy, Advanced Scientific Computing Research (ASCR) program in Applied

Mathematical Sciences.

References

[1] M. F. Abu-Taleb, The use of infiltration field tests for groundwater artificial recharge, Environ. Geol. 37 (1-2) (1999) 64–71.

[2] ASCE, Standard Guidelines for Artificial Recharge of Ground Water, Tech. rep., EWRI/ASCE 34-01 (ASCE Standard No. 34-01) (2001).

[3] M. Barahona-Palomo, D. Pedretti, X. Sanchez-Vila, Infiltration tests at the Sant Vicenç dels Horts artificial recharge experimental site, in: EGU General Assembly 2010 (ed.), Geophysical Research Abstracts, vol. 12 of EGU2010-5326, 2010.

[4] B. Batchelor, J. Valdes, V. Araganth, Stochastic risk assessment of sites contaminated by hazardous wastes, J. Environ. Eng. 124 (1998) 380–388.

[5] P. Baveye, V. A. Valocchi, An evaluation of mathematical models of the transport of biologically reacting solutes in saturated soils and aquifers, Water Resour. Res. 25 (6) (1989) 1413–1421.

[6] P. Baveye, P. Vandevivere, B. L. Hoyle, P. C. DeLeo, D. de Lozada-Sanchez, Environmental impact and mechanisms of the biological clogging of saturated soils and aquifer materials, Critical Rev. Environ. Sci. Tech. 28 (2) (1998) 123–191.

[7] T. Bedford, R. Cook, Probabilistic Risk Analysis: Fundations and methods, Cambridge University Press, New York, 2001.

[8] D. Bolster, M. Barahona-Palomo, M. Dentz, D. F. Garcia, X. Sanchez-Vila, P. Trinchero, C. Valhondo, D. M. Tartakovsky, Probabilistic risk assessment applied to contamination scenarios in porous media, Water Resour. Res. 45 (2009) W06413, doi:10.1029/2008WR007551.

[9] H. Bouwer, Artificial recharge of groundwater: hydrogeology and engineering, Hydrogeol. J.

[10] R. H. Boyd, M. M. Ghosh, An investigation of the influence of some physicochemical variables on porous-media filtration, J. Am. Water Works Assn. 66 (2) (1974) 94–98.

[11] R. H. Brooks, A. T. Corey, Hydraulic properties of porous media, Colorado St. Univ. Hydrol. Paper 3 (1964) 27.

[12] P. Carman, The determination of the specific surface of powders., J. Soc. Chem. Ind. Trans 57 (1938) 225.

[13] CGWB, Manual of artificial recharge of ground water, Tech. rep., Government of India. Ministry of water resources. Central Grond Water Board. New Delhi. (2007).

[14] Y.-I. Chang, W.-Y. C. , H.-C. Chan, A proposed correlation equation for predicting filter coefficient under unfavorable deposition conditions, Sep. Purif. Technol. 65 (3) (2009) 248–250.

[15] J. E. Christiansen, Effect of entrapped air upon the permeability of soils, Soil Sci. 58 (5) (1944) 355–366.

[16] F. Civan, Non-isothermal permeability impairment by fines migration and deposition in porous media including dispersive transport, Transp. Porous Med. (2010) doi:10.1007/s11242–010–9557–0.

[17] F. Civan, V. Nguyen, Modeling particle migration and deposition in porous media by parallel pathways with exchange, in: K. Vafai (ed.), Handbook of Porous Media, 2nd ed., CRC Press, Boca Raton, FL, 2005, pp. 457–484.

[18] F. Civan, M. L. Rasmussen, Analytical models for porous media impairment by particles in rectilinear and radial flows, in: K. Vafai (ed.), Handbook of Porous Media, 2nd ed., CRC Press, Boca Raton, FL, 2005, pp. 485–542.

[19] T. P. Clement, B. S. Hooker, R. S. Skeen, Macroscopic models for predicting changes in saturated porous media properties caused by microbial growth, Groundwater 34 (5) (1996) 934–942.

[20] F. P. J. de Barros, Y. Rubin, A risk-driven approach for subsurface site characterization, Water Resour. Res. 44 (2008) W01414.

[21] P. Dillon (ed.), Management of Aquifer Recharge for Sustainability: Proceedings of the 4th International Symposium on Artificial Recharge of Groundwater, Adelaide, Sep 2001., Taylor & Francis, New York, 2002 (2002).

[22] P. Dillon, Future management of aquifer recharge, Hydrogeol. J. 13 (1) (2005) 313–316.

[23] A. Drazen, E. Helpman, Economic effects on the government budgets, in: E. Helpman, A. Razin, E. Sadka (eds.), Stabilization with exchange rates management under uncertainty, chap. 16, MIT Press, Boston, 1998.

[24] V. A. Fry, J. D. Istok, L. Semprini, K. T. O'Reilly, T. E. Buscheck, Retardation of dissolved oxygen due to a trapped gas phase in porous media, Groundwater 33 (3) (1995) 391–398.

[25] J. Gomez-Hernandez, A. Journel, Joint sequential simulation of multi-Gaussian fields, in: A. Soares (ed.), Geostat Troia 1992, vol. 1, Kluwer, Dordrecht, Netherlands, 1993, pp. 85–94.

[26] J. Greskowiak, H. Prommer, G. Massmann, C. D. Johnston, G. Nützmann, A. Pekdeger, The impact of variable saturated conditions on the hydrochemistry during artificial recharge of groundwater – A field study, Appl. Geochem. 20 (2005) 1409–1426.

[27] A. Hazen, Some physical properties of sands and gravels, with special reference to their use in filtration, 24th Annual Rep., Massachusetts State Board of Health, Pub. Doc. 34 (1982) 539–556.

[28] T. Iwasaki, Some notes on sand filtration, J. Am. Water Works Assn. 29 (1937) 15971602.

[29] J. Kozeny, Uber kapillare leitung des wassers im boden, Sitzungsber. Akad. Wiss. Wien 136 (1927) 271–306.

[30] NRC, Ground Water Recharge Using Waters of Impaired Quality, Tech. rep., National Research Council, Committee on Ground Water Recharge, Water Science and Technology Board, Commission on Geosciences, Environment, and Resources., National Academy Press, Washington, D.C. (1994).

[31] NRC, Review of recommendations for probabilistic seismic hazard analysis: Guidance on uncertainty and use of experts, Tech. rep., National Research Council, Natl. Acad. Press, Washington, D.C. (1997).

[32] S. Orr, A. M. Meystel, Approaches to optimal aquifer management and intelligent control in a multiresolutional decision support system, Hydrogeol. J. 13 (1) (2005) 223–246.

[33] D. Pedretti, M. Barahona-Palomo, D. Bolster, D. Fernandez-Garcia, X. Sanchez-Vila, Quantitative assessment of the spatial distribution of infiltration capacity in soils using Google Earth images, Vadose Zone J.(under review).

[34] A. Perez-Paricio, Integrated model of clogging processes in artificial groundwater recharge, Ph.D. thesis, Department of Geotechnical Engineering and Geosciences, Technical University of Catalonia (UPC), Barcelona (2000).

[35] A. Perez-Paricio, J. Carrera, Clogging handbook., Tech. rep., Final report, EU project on Artificial Recharge of Groundwater. (1999).

[36] B. R. Scanlon, K. E. Keese, A. L. Flint, L. E. Flint, G. B. Gaye, W. M. Edmunds, I. Simmers, Global synthesis of groundwater recharge in semiarid and arid regions, Hydrol. Processes 20 (2006) 3335–3370.

[37] R. Smith, The infiltration envelope: results from a theoretical infiltrometer, Journal of Hydrology 17 (1972) 1–21.

[38] D. M. Tartakovsky, Probabilistic risk analysis in subsurface hydrology, Geophys. Res. Lett. 34 (2007) L05404, doi:10.1029/2007GL029245.

[39] D. M. Tartakovsky, C. L. Winter, Uncertain future of hydrogeology, ASCE J. 394 Hydrologic Engrg. 13 (1) (2008) 37–39.

[40] C. Tien, A. C. Payatakes, Advances in deep bed filtration, AIChE J. 25 (5) (1979) 737–759.

[41] N. Tufenkji, M. Elimelech, Correlation equation for predicting single-collector efficiency in physicochemical filtration in saturated porous media, Environ. Sci. Technol. 38 (2) (2004) 529–536.

[42] A. Tuinhof, J. P. Heederik (eds.), Management of aquifer recharge and subsurface storage. Netherlands National Committee - International Association of Hydrogeology, No. 4. NNCIAH Publication, 2003 (2003).

[43] M. T. van Genuchten, A closed-form equation for predicting hydraulic conductivity of unsaturated soils, Soil Sci. Soc. Am. J. 44 (1980) 892–898.

[44] P. Vandevivere, P. Baveye, D. S. de Lozada, P. DeLeo, Microbial clogging of saturated soils and aquifer materials: Evaluation of mathematical models, Water Resour. Res. 31 (9) (1995) 2173–2180.

[45] B. Wagner, S. Gorelick, Optimal groundwater quality management under parameter uncertainty, Water Resour. Res. 23 (7) (1987) 1162–1174.

[46] T. Wang, W. F. McTernan, The development and application of a multilevel decision analysis model for the remediation of contaminated groundwater under uncertainty, J. Environ. Manage. 64 (2002) 221–235.

[47] A. Zamani, B. Maini, Flow of dispersed particles through porous media – Deep bed filtration, J. Petrol. Sci. Eng. 69 (2009) 71–88.

[48] S. A. Zenios, R. M. Holmer, R. McKendall, C. Vassiadou-Zeniou, Dynamic models for fixed-income portfolio management under uncertainty., J. Econ. Dynam. Control 22 (10) (1998) 1517–1544.

[49] M. H. Zwietering, I. Jongenburger, F. M. Rombouts, K. van T Riet, Modeling of the bacterial growth curve, Appl. Environ. Microbiol. 56 (6) (1990) 1875–1881.